Generation and Detection of Pure Spin Current in an H-Shaped Structure of a Single Metal

Caigan Chen,[1,2,*] Dai Tian,[1,2,*] Hexin Zhou,[1,2] Dazhi Hou,[3] and Xiaofeng Jin[1,2,†]
[1]Department of Physics, State Key Laboratory of Surface Physics, Fudan University, Shanghai 200433, China
[2]Collaborative Innovation Center of Advanced Microstructures, Fudan University, Shanghai 200433, China
[3]WPI Advanced Institute of Materials Research, Tohoku University, Sendai 980-8577, Japan

(Received 28 June 2018; revised manuscript received 19 November 2018; published 9 January 2019)

Distinct from all the existing methods for determining the spin Hall angle with bilayers, we have developed a new approach based on the mesoscopic H-shaped structure, which generates and detects pure spin current in a single metal. Using this approach we have unequivocally addressed the long-standing controversy of the magnitude of the spin Hall angle of gold. By exploiting the long spin diffusion length of Cu and the large spin-orbit coupling of Bi, we have realized a very large spin Hall effect in 10 nm Cu films delta doped with 0.15 nm of Bi. This new artificial material can generate a large spin-orbit torque to switch an adjacent Fe layer. We have thus demonstrated new artificial materials with a simultaneously large spin Hall angle and long spin diffusion length.

DOI: 10.1103/PhysRevLett.122.016804

The spin Hall effect (SHE), where an unpolarized charge current gives rise to a pure spin current in the transverse direction, plays an important role in pure spin current phenomena and devices [1–4]. A key parameter in the SHE is the spin Hall angle (θ_H), which characterizes the conversion efficiency between the charge and the spin current. Thus far, four methods have been developed for exploring pure spin current: (1) nonlocal spin injection [5–7], (2) spin transfer torque [8,9], (3) spin pumping [10–12], and (4) spin Seebeck effect [13–16]. All of these approaches require a bilayer structure in which the spin current is generated in one material (usually a ferromagnetic material) and the converted charge current is detected in the other (usually a nonmagnetic metal with large spin-orbit coupling). However, one inevitably encounters complications in such bilayers due to interfaces of different materials and the shunting effect (if both materials are metals). These complications are the major contributing factors for the large variance of the reported θ_H values, even for the same combination of materials [17].

It is highly desirable to employ a method in which the spin current is generated and detected in one material, thus avoiding all the complications associated with the interfaces and shunting effect. The patterned mesoscopic H-shaped structure is, in principle, one such method [18,19], which Mihajlović *et al.* used to measure the SHE in gold (Au) [20]. Disappointingly, however, they failed to realize any measurable SHE signal in an H-shaped structure made of Au, in sharp contrast to the giant SHE reported by Seki *et al.* using a bilayer structure of FePt/Au [7]. These conflicting results cast doubt onto the value of θ_H for Au, if not the validity of the H-shaped method. In this Letter, we demonstrate for the first time the observation of the SHE and measurement of θ_H in Au using an H-shaped structure. The key to our success is the optimal dimensions necessary for accommodating the long spin diffusion length of Au.

One of the limiting factors for spintronics is the short spin diffusion length ($\lambda_s < 10$ nm) of most heavy metals with strong spin-orbit coupling and large θ_H (e.g., Pt and W). Materials with long λ_s, such as Cu and Ag, tend to have small θ_H. Consequently, most spintronics devices to date contain vertical structures, such as multilayers with small layer thicknesses. New materials with long λ_s and large θ_H can greatly expand the horizon of spintronics, such as lateral spintronics devices. Based on the characteristics of known materials, these conflicting demands are unlikely to be fulfilled in a single material. Accordingly, it is interesting to ask if it is possible to design new artificial materials, in which both the large spin-orbit coupling and long spin diffusion length can be realized.

In this Letter, we first show how to optimize the geometric parameters of the H-shaped structure specifically for Au thin films in order to extract the SHE contribution from others. We then demonstrate that the spin Hall angle (SHA) is indeed giant in 10 nm Au ($\theta_H > 10\%$) as declared by Seki *et al.*[7], yet negligible in 60 nm Au as found by Mihajlović *et al.* [20], thus unequivocally clarifying the long-standing controversy concerning the magnitude of the SHA of Au. Next, by combining the extremely long spin diffusion length of Cu and extremely large spin-orbit coupling of Bi, we have made an artificial metallic system by δ doping of Bi in Cu made by molecular beam epitaxy. The mesoscopic H-shaped measurement shows this artificial material exhibits simultaneously giant SHA ($\theta_H > 10\%$) and an extremely long spin diffusion length ($\lambda_s > 150$ nm), a feat never before

accomplished. To illustrate the giant SHE, we have realized current-driven magnetization switching of Fe thin film epitaxially grown on top of this artificial material. We thus demonstrate new artificial materials with a large SHA and long spin diffusion length.

Polycrystalline Au and Cu samples were prepared at 300 K by electron beam evaporation at a base pressure of 3×10^{-7} mtorr, and the devices were fabricated by electron-beam lithography (EBL) and standard lift-off process. Single crystalline Bi δ-doped Cu films were grown on MgO (111) in a molecular beam epitaxy chamber at 5×10^{-8} mtorr. First, the MgO (111) substrate was first annealed at 850 K for about 1 h until a sharp reflection high energy electron diffraction (RHEED) pattern was obtained. A 7 nm thick Cu film was then epitaxially grown on the MgO (111) substrate at 400 K, followed by a Bi δ-doping layer deposited on the Cu (111) epilayer at 110 K, then another 3 nm thick Cu film epitaxially grown on top. The deposition rate was controlled by a quartz microbalance. To prevent oxidation, a 4 nm MgO capping layer was finally deposited on Cu (delta doped by Bi) samples before it was taken out of vacuum. Thereafter, the Cu (delta doped by Bi) films were patterned into a mesoscopic H-shaped structure by EBL and Ar-ion beam etching. All the transport measurements were conducted in an Oxford cryo-free magnet system.

In an H-shaped structure, as shown in the left panel of Fig. 1(a), the unpolarized current injected at the left bar induces a pure spin current into the horizontal bar due to the SHE. The spin current further diffuses into the right arm and produces the charge accumulation via the inverse SHE

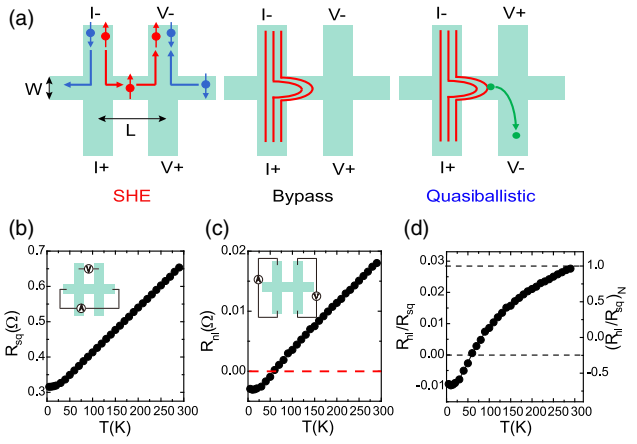

FIG. 1. (a) Schematic for three mechanisms in H-shaped measurement, the SHE, bypass effect, and quasiballistic are on the left, middle, and right, respectively. (b),(c) The sheet resistance R_{sq} and the nonlocal resistance R_{nl} as a function of temperature respectively, for Au(60 nm) with $L = 150$ nm and $W = 120$ nm. (d) The temperature dependence of reduced nonlocal resistance R_{nl}/R_{sq} is shown on the left scale. The right scale of normalized nonlocal signal $(R_{nl}/R_{sq})_N = (R_{nl}/R_{sq})_T/(R_{nl}/R_{sq})_{RT}$ shows the relative change from RT to low temperature.

(ISHE). This SHE-ISHE process gives a positive nonlocal resistance [19–21]

$$R_{nl}^{SHE} = \frac{1}{2} R_{sq} \theta_H^2 \frac{W}{\lambda_s} \exp\left(-\frac{L}{\lambda_s}\right), \tag{1}$$

where R_{sq} is the square resistance, θ_H is the SHA, λ_s is the spin diffusion length, W is the width of the horizontal bar, and L is the distance of the adjacent arms. However, in addition to the SHE, there are two other main effects involved in the nonlocal measurements, as shown in the middle and right panels of Fig. 1(a), respectively. These are the bypass resistance described by $R_{nl}^{by} = R_{sq} \exp[-(\pi L/W)]$, which provides a nonlocal voltage with the same polarity of the SHE, and the quasiballistic resistance by $R_{nl}^{qb} = -b \times R_{sq} \exp[-(\pi L/W)] \times \exp[-(W/l_e)]$, which provides a nonlocal voltage with the opposite polarity to the SHE, where l_e is the mean free path and b is a fitting parameter [20]. (More details can be found in the Supplemental Material [22].) Now the challenge becomes very obvious: extracting the SHE contribution from those of the bypass and quasiballistic, as detailed below.

Figures 1(b) and 1(c) present the sheet resistance R_{sq} and the nonlocal resistance R_{nl} as a function of temperature, respectively, for a 60 nm thick Au film with $L = 150$ nm and $W = 120$ nm. Both R_{sq} and R_{nl} decrease with reducing temperature. However, we can use the reduced nonlocal resistance R_{nl}/R_{sq} to exclude the temperature dependence of R_{sq} and examine more clearly the temperature dependence of the three nonlocal contributions. The SHE contribution R_{nl}^{SHE}/R_{sq} should increase for decreasing temperature due to longer λ_s at lower temperatures. In contrast, the bypass contribution R_{nl}^{by}/R_{sq} is temperature independent and only geometry related. Meanwhile, the quasiballistic contribution should also increase as temperature decreases due to the longer l_e at lower temperatures, but it is always of opposite sign to both the SHE and the bypass contributions. Figure 1(d) (left scale) presents the temperature dependence of the reduced nonlocal resistance R_{nl}/R_{sq} from Figs. 1(b) and 1(c), where R_{nl}/R_{sq} is positive at room temperature (RT), then decreases and becomes negative at lower temperatures. As mentioned above, the positive component of R_{nl} originates from the SHE and the bypass effect, while the negative component originates from the quasiballistic effect. As temperature decreases, the downward (R_{nl}/R_{sq})-T curve indicates the quasiballistic contribution becomes increasingly stronger and finally overwhelms the positive contribution from the SHE and bypass effect below 60 K. So far, there is no indication of the SHE, consistent with the result of Mihajlović *et al.* [20]. In order to visualize more explicitly the trends from different nonlocal contributions, we plot the normalized nonlocal signal $(R_{nl}/R_{sq})_N = (R_{nl}/R_{sq})_T/(R_{nl}/R_{sq})_{RT}$ in Fig. 1(d) (right scale) to show the relative change from RT to low temperature. Here, as temperature decreases from

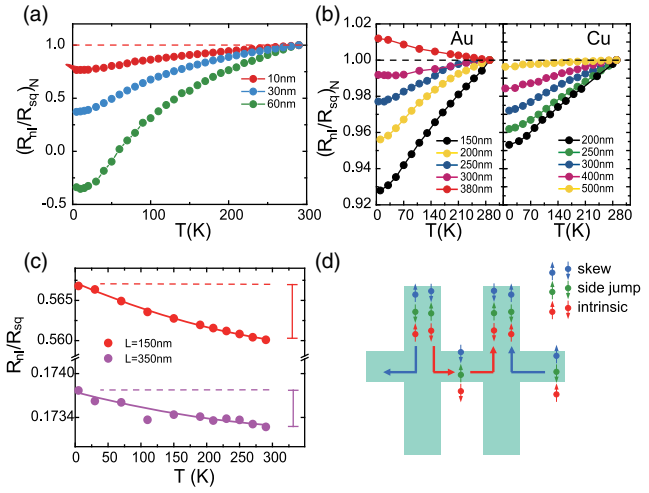

FIG. 2. (a) The $(R_{nl}/R_{sq})_N$-T curve for variant thickness Au films ($L = 150$ and $W = 120$ nm). (b) The $(R_{nl}/R_{sq})_N$-T curves for 10 nm Au films and 10 nm Cu films with variant W ($L = 150$ nm). (c) Nonlocal signal for 10 nm Au films with $W = 380$ nm but different L. (d) Schematic for extrinsic (skew in blue, side jump in green) and intrinsic (in red) scattering mechanisms in H-shaped measurement.

RT, the SHE shows an upward curve, the quasiballistic effect a downward curve, and the bypass contribution a flat curve.

In order to observe the SHE in Au, we tried first to reduce the thickness of Au film. By reducing the thickness, the interface scattering in Au films is enhanced; therefore, the quasiballistic effect is suppressed because of the shorter l_e. Figure 2(a) shows the $(R_{nl}/R_{sq})_N$-T curve for variant thickness Au films. All three curves are downward as temperature decreases, indicating that the quasiballistic effect still dominates. However, by reducing thickness from 60 to 10 nm, the downward tendency of the $(R_{nl}/R_{sq})_N$-T curve becomes increasingly weaker. This indicates that the contribution from the quasiballistic effect is indeed suppressed by reducing the thickness.

Even though the quasiballistic effect contribution is suppressed dramatically in the 10 nm thick Au film, the anticipated upward SHE is still missing in the downward $(R_{nl}/R_{sq})_N$-T curve. In order to obtain the unambiguous evidence of the SHE, i.e., the upward $(R_{nl}/R_{sq})_N$-T curve, we further optimized the geometry of the H-shaped structure to suppress the quasiballistic effect and enhance the SHE by varying the width W. Now, the left panel of Fig. 2(b) shows the $(R_{nl}/R_{sq})_N$-T curves for 10 nm Au films with various W. The $(R_{nl}/R_{sq})_N$-T curve finally changes from downward to upward when W is increased from 150 to 380 nm. For the sample with 380 nm width, the SHE is strong enough to overwhelm the quasiballistic effect and to make the $(R_{nl}/R_{sq})_N$-T curve upward. This upward $(R_{nl}/R_{sq})_N$-T curve unambiguously demonstrates the SHE in the 10 nm Au film with optimized geometry.

Actually, there is an optimized window of width to observe the upturn behavior. For a small width, the SHE signal is smaller than the quasiballistic. To observe an upturn behavior, we could enlarge the width W. When W is increased up to 400 nm, the SHE signal should be much larger than the quasiballistic. However, the bypass contribution is increasing much faster than the SHE contribution. The SHE signal will be overwhelmed for a width larger than 500 nm. To make a comparison, we have also measured the $(R_{nl}/R_{sq})_N$-T curve for 10 nm Cu films with various W, with the results shown in the right panel of Fig. 2(b). The quasiballistic effect is also suppressed when W is increased. However, the $(R_{nl}/R_{sq})_N$-T curve is always downward, showing no evidence of the SHE. This is readily explained by the negligible spin-orbit coupling in Cu.

To quantitatively determine the SHA for 10 nm Au film at low temperature, we measured the nonlocal signal for Au films with $W = 380$ nm but different L, as shown in Fig. 2(c). Here, the quasiballistic effect is overwhelmed by the SHE and can be neglected. Therefore, we can get $(R_{nl}/R_{sq}) = (R_{nl}^{SHE}/R_{sq}) + (R_{nl}^{by}/R_{sq})$. If we further take the residual negative quasiballistic contribution into account, the actual value of the spin Hall signal would be even larger. Considering the fact that R_{nl}^{by}/R_{sq} is temperature independent, we can exclude the bypass contribution by subtracting $(R_{nl}/R_{sq})_{RT}$ from $(R_{nl}/R_{sq})_{5K}$ and get $\Delta(R_{nl}/R_{sq}) = (R_{nl}^{SHE}/R_{sq})_{5\,K} - (R_{nl}^{SHE}/R_{sq})_{RT}$, thus

$$\Delta\frac{R_{nl}}{R_{sq}} = \frac{1}{2}(\theta_H^{5\,K})^2\frac{W}{\lambda_s^{5\,K}}\exp\left(-\frac{L}{\lambda_s^{5\,K}}\right) - \frac{1}{2}(\theta_H^{RT})^2\frac{W}{\lambda_s^{RT}}\exp\left(-\frac{L}{\lambda_s^{RT}}\right), \quad (2)$$

where $\theta_H^{5\,K}$ and $\lambda_s^{5\,K}$ are the SHA and spin diffusion length at 5 K, and θ_H^{RT} and λ_s^{RT} are the SHA and spin diffusion length at RT. In general, λ_s^{RT} is much smaller than $\lambda_s^{5\,K}$ [28–30]; therefore, $(R_{nl}^{SHE}/R_{sq})_{RT}$ can be neglected in Eq. (2). If we take the RT term $(R_{nl}^{SHE}/R_{sq})_{RT}$ into account, the actual value of θ_H^{5K} would be even larger. By substituting the effective length L_{eff} (see the Supplemental Material, Sec. S1 [22–27]) at 150 and 350 nm, we get $\theta_H^{5K} = 0.10 \pm 0.01$ and $\lambda_s^{5K} = 77 \pm 5$ nm, which demonstrates a giant SHE in Au.

We have demonstrated the giant SHA and a moderate spin diffusion length in Au, resolving a long-standing controversy. However, is it possible to achieve both a giant SHA and a long spin diffusion length in the same material as a superior spintronics material should be? By combining the extremely long spin diffusion length of Cu and the extremely large spin-orbit coupling of Bi, we have realized a desirable material with both attributes in epitaxial Cu film delta doped by Bi. The epitaxial Cu films delta doped by Bi exploits the long spin diffusion length of Cu and the strong

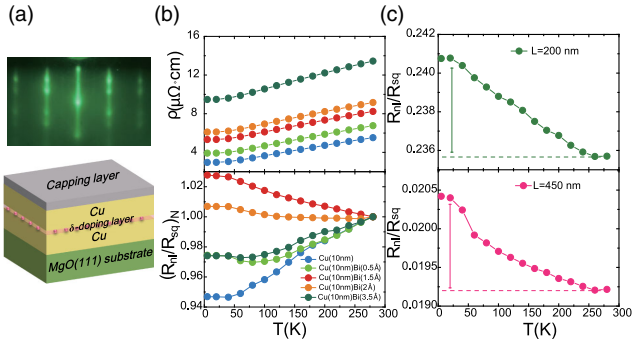

FIG. 3. (a) The RHEED pattern and structure illustration of the single crystal Cu films delta doped by Bi. (b) (upper) The effect of Bi doping on the resistivity of Cu and (lower) $(R_{\rm nl}/R_{\rm sq})_N$-$T$ curves for samples with variant Bi doping level. (c) Nonlocal signal for 10 nm Cu films delta doped by 1.5 Å Bi with $W =$ 400 nm but different L.

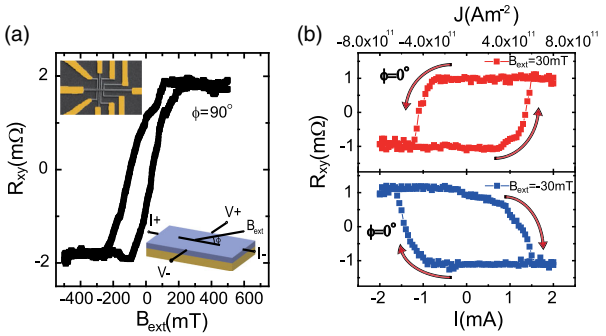

FIG. 4. (a) The AHE of Fe(0.8 nm)/Cu(3 nm)/Bi(0.15 nm)/Cu(7 nm)/MgO(111) at 2 K. The current-driven magnetization switching is shown in (b). The anomalous Hall resistance is measured for variant current under an in-plane magnetic field $B_{\rm ext}$ ($\phi = 0°$).

spin-orbit coupling of Bi impurities, far better than previous CuBi alloys [31–33].

Figure 3(a) shows the RHEED pattern and structure illustration of epitaxial Cu films delta doped by Bi. The effect of Bi doping on the resistivity of Cu is shown in the upper panel of Fig. 3(b). The resistivity increases more than three times as the Bi doping level increases from 0 to 3.5 Å, which indicates the scattering due to Bi impurities plays a crucial role in the electrical transport. The lower panel of Fig. 3(b) shows $(R_{\rm nl}/R_{\rm sq})_N$-$T$ curves for samples with various Bi doping levels. The data of 10 nm pure Cu show a downward curve indicating the quasiballistic effect. By introducing only 0.5 Å Bi, the curve moves upward, which means the SHE is competing with the quasiballistic effect. More surprisingly, a clear upward curve is observed when there is only 1.5 Å Bi doped. This upward $(R_{\rm nl}/R_{\rm sq})_N$-$T$ curve demonstrates that the SHE is realized in the Cu films delta doped by Bi. However, if we further dope Bi atoms, there is a suppression of the SHE, making the $(R_{\rm nl}/R_{\rm sq})_N$-$T$ curve downward again. The doped Bi atoms introduce very strong spin-orbit coupling, which causes the observed SHE. However, excess Bi atoms may tend to form small clusters. These clusters behave like bulk Bi, in which there is negligible SHE [34]. This may explain why there is a suppression of the SHE in overdoped samples. We also measure $R_{\rm nl}/R_{\rm sq}$ for samples with different $L_{\rm eff}$ to calculate the SHA and spin diffusion length [Fig. 3(c)] and get $\theta_H^{5\,\rm K} = 0.12 \pm 0.01$ and $\lambda_s^{5\,\rm K} = 170 \pm 12$ nm. The results show both giant SHA and extremely long spin diffusion length.

As is well known, the spin-orbit torque from a strong SHE can be used to switch the magnetization of a ferromagnetic layer [8]. Here we have succeeded in switching the magnetization of an Fe layer using the giant SHE of Cu delta doped by Bi. Figure 4(a) shows the anomalous Hall effect (AHE) measurement of Fe(0.8 nm)/Cu(3 nm)/Bi(0.15 nm)/Cu(7 nm)/MgO(111) at 2 K. The squarelike loop indicates that the ultrathin Fe film has perpendicular magnetic anisotropy, consistent with the previous report [35]. The current-driven magnetization switching is shown in Fig. 4(b). The anomalous Hall resistance is measured for various currents under an in-plane magnetic field $B_{\rm ext}$ ($\phi = 0°$). In order to avoid the heating effect, for each data point, a large current pulse is applied for 0.2 s first, then the anomalous Hall resistance R_{xy} is measured by a much smaller current (100 μA). The $R_{xy} - I$ loops unambiguously show the current-driven magnetization switching effect. The critical current density for magnetization switching is about 5×10^{11} A/m^2. The $R_{xy} - I$ loop changes from counterclockwise to clockwise when $B_{\rm ext}$ changes from positive to negative, consistent with the spin-orbit torque origin [8]. According to the switching direction, the SHA of Cu delta doped by Bi is negative, the same as the former report [33].

Finally, it should be noted that the SHE is a special case of the AHE, in which the carrier densities of spin-up and spin-down are identical [36]. So, there are also three mechanisms in the SHE, including skew scattering, side jump, and intrinsic, which leads to $\rho_{xy}^{\rm SHE} = \rho_{xy}^{\rm skew} + \rho_{xy}^{\rm side\ jump} + \rho_{xy}^{\rm intrinsic}$ [37,38]. Usually, the signs of the three terms could be different, which may lead to a cancellation of spin accumulation, similar to the sign change of the AHE of Fe as a function of temperature [39]. However, the nonlocal SHE signal measured here by the H-shaped structure results from the SHE-ISHE process [Fig. 2(d)], so $\rho_{\rm nl}^{\rm SHE-ISHE} = |\rho_{\rm nl}^{\rm skew}| + |\rho_{\rm nl}^{\rm side\,jump}| + |\rho_{\rm nl}^{\rm intrinsic}|$. That means, even though the signs of the three terms are different, their contributions to the SHE signal measured by the H-shaped structure are constructively added. Therefore, the H-shaped structure measurement is a good method to magnify the SHE and could be useful for lateral spintronics devices.

In conclusion, we have unequivocally addressed the long-standing controversy of the magnitude of the SHA of gold and established a new method to evaluate the SHA at the lower limit. To achieve a highly effective SHE, we

introduce giant spin-orbit coupling in Cu films delta doped by Bi. The nonlocal H-shaped measurements reveal the giant SHE of Cu films delta doped by Bi, which executes electric-current-driven magnetization switching. We realize a giant SHE in Cu, while maintaining its long spin diffusion length, which sheds light on possible applications of this type of artificial material.

This work is supported by National Nature Science Foundation of China (NSFC) (Grants No. 2015CB921402, No. 11374057, No. 11434003, No. 11421404 and No. 2016YFA0300703).

*These two authors contributed equally.
†Corresponding author.
xfjin@fudan.edu.cn

[1] C. G. Shull, C. T. Chase, and F. E. Myers, Phys. Rev. **63**, 29 (1943).
[2] M. I. Dyakonov and V. I. Perel, JETP Lett. **13**, 467 (1971).
[3] J. E. Hirsch, Phys. Rev. Lett. **83**, 1834 (1999).
[4] J. Sinova, S. O. Valenzuela, J. Wunderlich, C. H. Back, and T. Jungwirth, Rev. Mod. Phys. **87**, 1213 (2015).
[5] S. O. Valenzuela and M. Tinkham, Nature (London) **442**, 176 (2006).
[6] T. Kimura, Y. Otani, T. Sato, S. Takahashi, and S. Maekawa, Phys. Rev. Lett. **98**, 156601 (2007).
[7] T. Seki, Y. Hasegawa, S. Mitani, S. Takahashi, H. Imamura, S. Maekawa, J. Nitta, and K. Takanashi, Nat. Mater. **7**, 125 (2008).
[8] L. Liu, C.-F. Pai, Y. Li, H. W. Tseng, D. C. Ralph, and R. A. Buhrman, Science **336**, 555 (2012).
[9] C.-F. Pai, L. Liu, Y. Li, H. W. Tseng, D. C. Ralph, and R. A. Buhrman, Appl. Phys. Lett. **101**, 122404 (2012).
[10] E. Saitoh, M. Ueda, H. Miyajima, and G. Tatara, Appl. Phys. Lett. **88**, 182509 (2006).
[11] K. Ando, Y. Kajiwara, S. Takahashi, S. Maekawa, K. Takemoto, M. Takatsu, and E. Saitoh, Phys. Rev. B **78**, 014413 (2008).
[12] O. Mosendz, J. E. Pearson, F. Y. Fradin, G. E. W. Bauer, S. D. Bader, and A. Hoffmann, Phys. Rev. Lett. **104**, 046601 (2010).
[13] K. Uchida, K. Takahashi, K. Harii, J. Ieda, W. Koshibae, S. Maekawa, and E. Saitoh, Nature (London) **455**, 778 (2008).
[14] T. Kikkawa, K. Uchida, Y. Shiomi, Z. Qiu, D. Hou, D. Tian, H. Nakayama, X.-F. Jin, and E. Saitoh, Phys. Rev. Lett. **110**, 067207 (2013).
[15] S. Y. Huang, W. G. Wang, S. F. Lee, J. Kwo, and C. L. Chien, Phys. Rev. Lett. **107**, 216604 (2011).
[16] D. Qu, S. Y. Huang, J. Hu, R. Wu, and C. L. Chien, Phys. Rev. Lett. **110**, 067206 (2013).
[17] S. Maekawa, S. O. Valenzuela, E. Saitoh, and T. Kimura, *Spin Current* (Oxford Science Publications, Oxford, 2011), pp. 2004–2005.
[18] E. M. Hankiewicz, L. W. Molenkamp, T. Jungwirth, and J. Sinova, Phys. Rev. B **70**, 241301 (2004).
[19] D. A. Abanin, A. V. Shytov, L. S. Levitov, and B. I. Halperin, Phys. Rev. B **79**, 035304 (2009).
[20] G. Mihajlović, J. E. Pearson, M. A. Garcia, S. D. Bader, and A. Hoffmann, Phys. Rev. Lett. **103**, 166601 (2009).
[21] D. Tian, C. C. Chen, H. Wang, and X. J. Jin, Chin. Phys. B **25**, 107201 (2016).
[22] See Supplemental Material at http://link.aps.org/supplemental/10.1103/PhysRevLett.122.016804 for more detailed description of quantitative analysis based on the H-shaped method, which includes Refs. [23–27].
[23] J. R. Sánchez, L. Vila, G. Desfonds, S. Gambarelli, J. P. Attané, J. M. D. Teresa, C. Magén, and A. Fert, Nat. Commun. **4**, 2944 (2013).
[24] K. Shen, G. Vignale, and R. Raimondi, Phys. Rev. Lett. **112**, 096601 (2014).
[25] S. Karube, K. Kondou, and Y. Otani, Appl. Phys. Express **9**, 033001 (2016).
[26] H. Bentmann, T. Kuzumaki, G. Bihlmayer, S. Blügel, E. V. Chulkov, F. Reinert, and K. Sakamoto, Phys. Rev. B **84**, 115426 (2011).
[27] L. Liu, T. Moriyama, D. C. Ralph, and R. A. Buhrman, Phys. Rev. Lett. **106**, 036601 (2011).
[28] R. J. Elliott, Phys. Rev. **96**, 266 (1954).
[29] T. Kimura, T. Sato, and Y. Otani, Phys. Rev. Lett. **100**, 066602 (2008).
[30] Y. Ji, A. Hoffmann, J. S. Jiang, and S. D. Bader, Appl. Phys. Lett. **85**, 6218 (2004).
[31] M. Gradhand, D. V. Fedorov, P. Zahn, and I. Mertig, Phys. Rev. B **81**, 245109 (2010).
[32] M. Gradhand, D. V. Fedorov, P. Zahn, and I. Mertig, Phys. Rev. Lett. **104**, 186403 (2010).
[33] Y. Niimi, Y. Kawanishi, D. H. Wei, C. Deranlot, H. X. Yang, M. Chshiev, T. Valet, A. Fert, and Y. Otani, Phys. Rev. Lett. **109**, 156602 (2012).
[34] D. Hou, Z. Qiu, K. Harii, Y. Kajiwara, K. Uchida, Y. Fujikawa, H. Nakayama, T. Yoshino, T. An, K. Ando, X. Jin, and E. Saitoh, Appl. Phys. Lett. **101**, 042403 (2012).
[35] J. Shen, R. Skomski, M. Klaua, H. Jenniches, S. S. Manoharan, and J. Kirschner, Phys. Rev. B **56**, 2340 (1997).
[36] D. Yue and X. Jin, J. Phys. Soc. Jpn. **86**, 011006 (2017).
[37] Y. Tian, L. Ye, and X. Jin, Phys. Rev. Lett. **103**, 087206 (2009).
[38] D. Hou, G. Su, Y. Tian, X. Jin, S. A. Yang, and Q. Niu, Phys. Rev. Lett. **114**, 217203 (2015).
[39] P. N. Dheer, Phys. Rev. **156**, 637 (1967).